I&EC research
Industrial & Engineering Chemistry Research
pubs.acs.org/IECR
Article

Antiscaling Evaluation and Quantum Chemical Studies of Nitrogen-Free Organophosphorus Compounds for Oilfield Scale Management

Mohamed F. Mady,* Safwat Abdel-Azeim, and Malcolm A. Kelland

Cite This: *Ind. Eng. Chem. Res.* 2021, 60, 12175−12188

Read Online

ACCESS | Metrics & More | Article Recommendations | Supporting Information

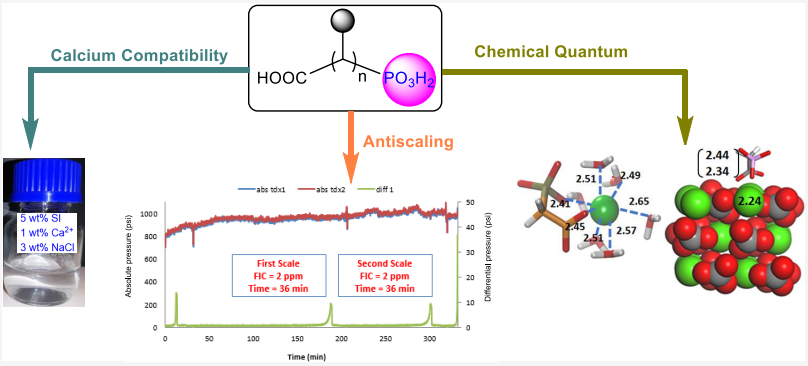

ABSTRACT: Nonpolymeric aminomethylenephosphonates are widely used as powerful scale inhibitors in the petroleum industry. However, most of these inhibitors have certain drawbacks, such as low biodegradability and incompatibilities with high calcium brines. Therefore, there is a great need to explore more biodegradable phosphonated oilfield scale inhibitors affording high calcium-ion tolerance. In this project, known and new nitrogen-free phosphonates have been tested as scale inhibitors against carbonate and sulfate scales according to the Heidrun oilfield, Norway. The considered nitrogen-free scale inhibitors are 1,2,4-phosphonobutanetricarboxylic acid (**PBTCA**), hydroxyphosphonoacetic acid (**HPAA**), phosphonoacetic acid (**PAA**), and 3-phosphonopropanoic acid (**PPA**). A high-pressure dynamic tube-blocking test, calcium tolerance, thermal aging, and seawater biodegradation were used to assess the antiscaling performance of these inhibitors. A very good to excellent performance of all nitrogen-free phosphonate scale inhibitors has been observed against the calcite scaling. A biodegradable naturally occurring **PAA** displayed a very good calcite inhibition efficiency and afforded excellent thermal stability at 130 °C for 7 days under anaerobic conditions. **PAA** also gave outstanding tolerance activity with all concentrations up to 10 000 ppm calcium ions. Density functional theory (DFT) simulations predicted higher affinities of the commercial SIs compared to the nitrogen-free molecules, which is in line with their calcium compatibilities. The high calcium tolerance of nitrogen-free molecules makes them more efficient than commercial inhibitors. Further, DFT solid-state simulations reveal that the affinities of the nitrogen-free molecules for the calcite surface are higher than the barite surface, which agrees well with the experimental fail inhibitor concentration (FIC) data. The sluggish and complicated kinetics of the barite scale formation compared to the calcite scale explain well the high concentrations of the nitrogen-free molecules required for barite inhibition. In summary, our results showed that the nitrogen-free molecules show good potential as scale inhibitors for both calcite and barite. However, for the latter scale, further optimization is needed for optimal performance.

1. INTRODUCTION

Organophosphorus compounds have been attracting extensive attention for many decades because of their widespread and vast industrial and medical applications.[1−3] Many of these chemicals have been used across various applications in the petroleum industry, particularly for hydrocarbon production.[4] Oilfield scaling is a significant problem in the petroleum industry. Calcium carbonate ($CaCO_3$, calcite) and barium sulfate ($BaSO_4$, barite) are common types of sparingly soluble inorganic salts in the oilfield industry.[4,5] There is a clear need to quickly tackle the scale formation to avoid formation damage or blocking conduits.

Organophosphorus-based scale inhibitors (SIs) are considered the most typical chemicals for oilfield scale management, mainly to prevent calcite and barite scaling. These chemicals work by inhibiting either crystal growth and/or nucleation of

Received: June 23, 2021
Revised: August 4, 2021
Accepted: August 9, 2021
Published: August 17, 2021

https://doi.org/10.1021/acs.iecr.1c02441
Ind. Eng. Chem. Res. 2021, 60, 12175−12188

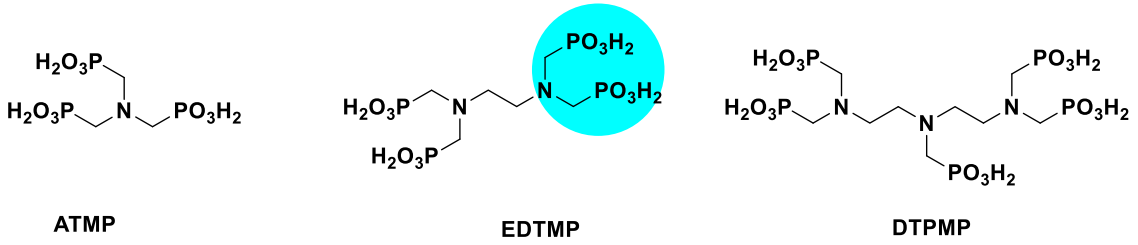

Figure 1. Commerical oilfield scale inhibitors containing aminomethylenephosphonate groups.

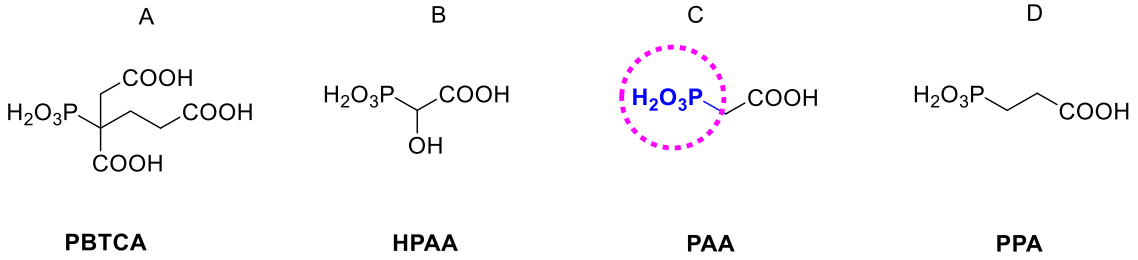

Figure 2. Structures of nitrogen-free phosphonates as oilfield scale inhibitors. From left: 1,2,4-phosphonobutanetricarboxylic acid (**PBTCA**), hydroxyphosphonoacetic acid (**HPAA**), phosphonoacetic acid (**PAA**), and 3-phosphonopropanoic acid (**PPA**).

inorganic scales.[6] Especially, phosphonic acid derivatives ($-C-PO(OH)_2$) are widely used as oilfield SIs. The phosphonate moiety improves adsorption/desorption properties onto formation rock in squeeze treatment applications, allowing the inhibitor to be retained in the petroleum reservoir and leading to a prolonged scale inhibition lifetime.[7] In addition, it is well-known that the concentration of phosphonate-based SIs can be easily monitored in the produced water using various techniques such as inductively coupled plasma mass spectrometry and high-pressure liquid chromatography compared to nonphosphonated SIs.[8]

Polymeric and nonpolymeric aminomethylenephosphonates ($-RR'-N-CH_2-PO_3H_2$) are well-known commercial oilfield SIs and have been widely applied in the upstream oil and gas industry for decades.[9] These chemicals were generally synthesized by phosphonation of the amine groups via the Irani–Moedritzer and/or the Kabachnik–Fields reactions.[10] Figure 1 shows some of the commercial oilfield SIs containing aminomethylenephosphonate groups, such as aminotrismethylenephosphonic acid (**ATMP**), ethylenediaminetetra methylenephosphonic acid (**EDTMP**), and diethylenetriaminepentamethylenephosphonic acid (**DTPMP**).

Aminomethylenephosphonate-based SIs showed excellent scale inhibition performance for both carbonate and sulfate scales, particularly for high-pressure, high-temperature (HPHT) applications.[11] It was found that the aminomethylenephosphonate moiety improves the metal-binding activities of the SI by the chelation of both the amine nitrogen and phosphonate oxygen atoms. However, most of these chemicals showed certain drawbacks, such as low biodegradability and incompatibilities with high calcium brines. Thus, several research groups have attempted to develop more environmentally friendly and calcium-compatible oilfield scale inhibitors containing phosphonate groups.[12−19]

Nitrogen-free phosphonate SIs have been developed and utilized in the petroleum industry.[4] However, a few chemicals have been developed to be useful for oilfield scale management. 1,2,4-Phosphonobutanetricarboxylic acid (**PBTCA**) is a rare class of an oilfield SI, particularly for calcite scaling.[20] **PBTCA** contains one phosphonic acid and three carboxylic acid groups on its backbone, as shown in Figure 2A. Another class of nitrogen-free phosphonate-based SIs is hydroxyphosphonoacetic acid (**HPAA**). **HPAA** consists of one phosphonic acid, one carboxylic acid, and one hydroxyl group in the structural backbone (Figure 2B). It was reported that **HPAA** can be used as a scale and corrosion inhibitor for industrial cooling water systems.[21,22] However, very little information on the scale inhibition performance of **HPAA** at oilfield conditions can be found in the open literature.

Phosphonoacetic acid (**PAA**) has attracted significant attention for biomedical applications. **PAA** has been used as an antiviral agent with inhibition activities against several viruses such as herpes simplex, Epstein-Barr, vaccinia, equine abortion, and avian herpes virus. It was also reported that **PAA** is widely utilized as a promising inhibitor of DNA polymerase δ.[23] **PAA** is a simple nitrogen-free phosphonate compound that includes one phosphonic acid and one carboxylic acid group. **PAA** can be presented as a phosphonate-end-capped alkane (methane)-1-carboxylic acid, as shown in Figure 2C.

In continuation of our research program focused on developing biodegradable SIs bearing the phosphonic acid moiety, **PAA** can be proposed and evaluated as a green alternative for commercial aminomethylenephosphonate oilfield SIs. Furthermore, 3-phosphonopropanoic acid (**PPA**) is a close analogue of **PAA**, consisting of phosphonate-end-capped alkane (ethane)-1-carboxylic acid, as presented in Figure 2D.

To the best of our knowledge, there are no studies in the open literature on the dynamic scale inhibition performance for these classes of nitrogen-free phosphonate-based SIs (Figure 2A–D) for calcite and barite scaling at harsh oilfield conditions, such as high-pressure high-temperature (HPHT) petroleum reservoirs. Herein, we report the dynamic scale inhibition performances for a series of nitrogen-free phosphonates (**PBTCA**, **HPAA**, **PAA**, and **PPA**) for calcite and barite scaling compared to two commercial aminomethylenephosphonate SIs **ATMP** and **DTPMP** using a high-pressure dynamic tube-blocking rig at 80 bar and 100 °C according to the Heidrun oilfield, Norway. Furthermore, we report the seawater biodegradabilities of all SIs. We also studied the calcium compatibility and thermal stability of the

https://doi.org/10.1021/acs.iecr.1c02441
Ind. Eng. Chem. Res. 2021, 60, 12175−12188

potentially biodegradable SI (**PAA**) at 130 °C for 1 week under anaerobic conditions. Moreover, we performed density functional theory (DFT) simulations to examine the metal affinities of the considered SIs. We aim to gain detailed atomic insights into the molecular interactions that govern the inhibition mechanism of these molecules.

2. EXPERIMENTAL SECTION

2.1. Chemicals. All reagents and solvents were purchased from VWR, Tokyo Chemical Industry Co., Ltd., and Sigma-Aldrich (Merck) and used as received. Phosphonoacetic acid (**PAA**) and 3-phosphonopropanoic acid (**PPA**) were purchased from Tokyo Chemical Industry Co., Ltd. Aminotrismethylenephosphonic acid (**ATMP**), diethylenetriaminepentamethylenephosphonic acid (**DTPMP**), and 1,2,4-phosphonobutanetricarboxylic acid (**PBTCA**) were supplied by Italmatch Chemicals S.p.A. Italy. Hydroxyphosphonoacetic acid (**HPAA**) was obtained from ShanDong XinTai Water Treatment Technology Co., Ltd., China.

2.2. High-Pressure Dynamic Tube-Blocking Test Methods. High-pressure dynamic tube-blocking experiment is a reasonable and efficient laboratory procedure that screens the scale inhibition performance of different chemicals for oilfield scales. In this report, a high-pressure dynamic tube-blocking scale rig produced by Scaled Solutions Ltd. (U.K.) was utilized to screen the inhibition efficiency performance of all tested organophosphorus-compound-based SIs. The dynamic scale rig consisted of three pumps, as presented in Figure S1. Each pump flushes solution up to 10.00 mL/min via a 316 stainless steel coil with a 1 mm diameter and 3.00 m length. The microbore coil is located inside an oven. Generally, the test was carried out at 100 °C and 80 bar for oilfield scale control, as described previously in our articles.[12−18]

The main features of the three pumps are described herein as follows: pump 1: flushing brine 1 of scaling cations (formation water) with a constant flow rate of 5.00 mL/min; pump 2: flushing brine 2 of scaling anions (seawater). We also used pump 2 to flush the cleaning mixture solutions containing a high alkaline aqueous solution of tetrasodium ethylenediaminetetraacetate (Na_4EDTA 5 wt %) and distilled water, separately; pump 3: flushing various programmed inhibitor concentrations. The tested SI (1000 ppm) was prepared in 500 mL of distilled water at similar reservoir pH values. Therefore, we adjusted all tested SI solutions at pH 4−6 according to the Heidrun oilfield, North Sea, Norway. In addition, the water compositions of both brine used in this project were adjusted according to the Heidrun oilfield, as shown in Table 1. Table 1 shows a 1:1 volume mixture of synthetic seawater and produced water to form the oilfield barite scale, except for bicarbonate (HCO_3^-) ions. Both brines were freshly prepared for each test and then degassed using a vacuum pump to remove gases and bubbles through the tubing.

Table 1. Reservoir Water Chemical Composition of the Heidrun Oilfield, Norway

ion	Heidrun formation water (ppm)	seawater (ppm)	50/50 mixed brine (ppm)
Na^+	19 500	10 900	15 200
Ca^{2+}	1020	428	724
Mg^{2+}	265	1368	816
K^+	545	460	502
Ba^{2+}	285	0	142
Sr^{2+}	145	0	72
SO_4^{2-}	0	2960	1480
HCO_3^-	880	120	500

The obtained results from the high-pressure dynamic tube-blocking test afford the minimum inhibitor concentration (MIC) and the fail inhibitor concentration (FIC). The FIC means that the tested inhibitor loses its efficiency to prevent scale formation. The MIC can refer to the inhibitor, which prevents oilfield scale formation. In general, the tested concentrations of our new SIs against oilfield scales were started at 100 ppm and dropped to 50, 20, 10, 5, 2, and, finally, 1 ppm over the 1 h test period or until oilfield scales were precipitated in the 316 stainless steel (SS316) coil.

After the dynamic tube-blocking experiments of the tested inhibitors are conducted, the obtained results were collected from a computer with LabView 8.0 software and then were exported to an Excel file. Excel provides a plot graph of the scaling time in minutes versus the differential pressure (psi) over the coil. This plot shows four stages for each test, as follows: the first blank test, the first scale test, the second scale test, and finally, a new second blank test.

2.3. Thermal Aging Test. The long-term thermal stability test procedure specifically gives how a chemical performs at elevated temperatures according to the high-pressure high-temperature (HPHT) petroleum reservoirs. A 5.0 wt % solution of the tested SI was prepared in 20 mL of distilled water (pH = 4−4.5). The mixture medium was transferred into a pressure tube and was purged with nitrogen gas for 1 h to remove dissolved oxygen gas. The purged sealed tube was then heated at 130 °C for 1 week. Samples of the aged solution were then screened for oilfield scales (calcite and barite) compared to the unaged chemical using the dynamic scale loop test procedure.

2.4. OECD 306 Seawater Biodegradation Test. Laboratory seawater biodegradation tests were carried out for all tested aminomethylenephosphonate and nitrogen-free phosphonate SIs using the Organisation for Economic Development and Co-operation (OECD, ISO) standard test method.[24] In this project, we have used the OECD 306 procedure to determine the biodegradation activities of the SIs in seawater. It is well-known that this biodegradability experiment is an important test to approve the Oslo and Paris (OSPAR) Commission regulations for discharging chemicals in the marine environment. In general, the OECD test measures the complex biochemical process that operates when microorganisms consume the tested chemical. This experiment indicates the biodegradability activity of the tested compound depending on the amount of carbon available for microbial consumption. Furthermore, the test procedure detects carbon dioxide production, oxygen consumption, and the concentration of inorganic carbon (IC) present in the sample.[25]

Generally, biological oxygen demand (BOD) of the tested SI was detected using the OxiTop Control manometric system (WTW, Germany) over a 28 day period. The percentages of BOD activity were calculated by comparing the measured BOD of SI with calculated theoretical oxygen demand (ThOD) values. Seawater was utilized as the experiment medium, and nutrients were added to the mixture to ensure suitable conditions for microbial activity and growth. It is also

https://doi.org/10.1021/acs.iecr.1c02441
Ind. Eng. Chem. Res. 2021, 60, 12175−12188

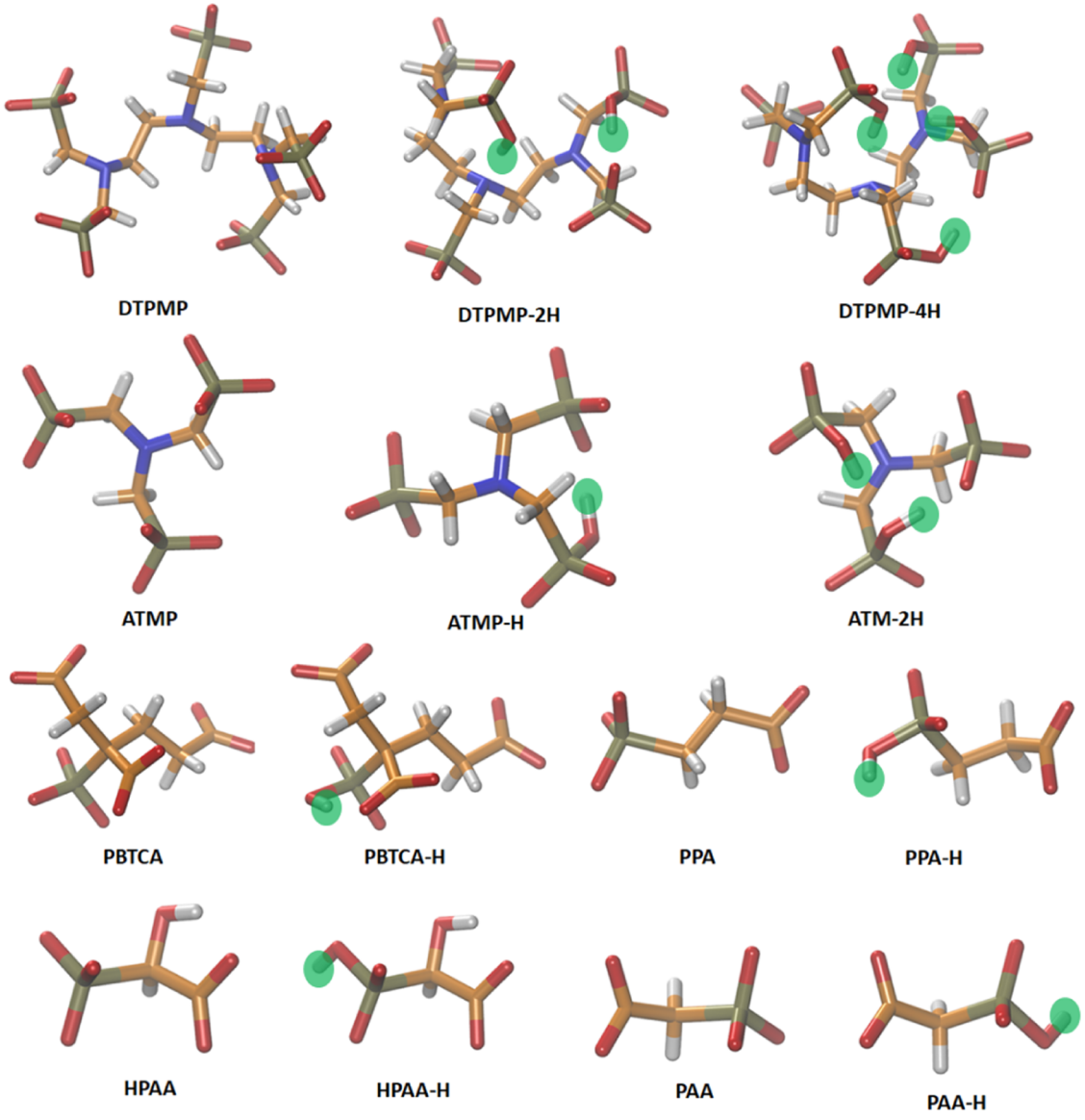

Figure 3. Optimized structures of all of the scale inhibitors considered in our study at two pH values (6, 10) are shown in sticks. Color code: C, orange; O, red; N, blue; P, olive; and H, white. The added protons are marked by green spheres.

crucial to autoclave all test vessels to avoid any bacterial contamination.

The in-house OECD 306 biodegradation test procedure has been illustrated several times in our published articles previously.[12,14] Test vessels were filled with seawater, SI, nutrients, and three different classes of control vessels. Control vessels contained the (1) blank with nutrient-modified seawater only; (2) negative control containing autoclaved seawater, nutrients, and the SI (69 mg/L); and (3) positive control with nutrient-modified seawater including sodium benzoate (100 mg/L), as the biodegradable standard ref 12.

The seawater applied in the BOD experiments (20 L) was collected at the NORCE Norwegian Research Centre AS in Mekjarvik (near Stavanger, Norway). The temperature of the collected seawater was 12 °C on the sampling day. This water was immediately kept in a dark room at 20 °C overnight. The next day, the seawater (297 mL) was transferred into 510 mL volume flasks, and the nutrient mixture solution was then added. The OxiTop control system was adjusted based on the recommendations of the supplier. In addition, all test vessels with self-check measurement heads were incubated for 3 h at 20 °C. After that, 1.8 mL of a 1.0% (w/w) solution (in deionized water) of each SI was transferred to the test mixture and negative control vessels, while 1.0 mL of a 30 g/L sodium benzoate solution was transferred to the positive control vessel. The vessels were covered with measuring heads and located in the incubator cabinet under stirring. The measuring heads were started immediately. The complete data and results of the oxygen consumption were collected after 28 days. ThOD of the tested SI was calculated as illustrated in the OECD 306 protocol. The biodegradability percentage of each SI was measured after deducting blank oxygen consumption values.

2.5. Formation Water and Seawater Compatibility Test. The aim of the compatibility test is to detect the tolerance performance of SIs with oilfield waters (seawater and formation water) in the petroleum reservoir. It is well-known that most produced oilfield water includes high total dissolved solid (TDS) brine, especially calcium ions. When the SIs are dissolved in the waters, this can cause precipitation of insoluble compounds, leading to formation damage and weak adsorption

https://doi.org/10.1021/acs.iecr.1c02441
Ind. Eng. Chem. Res. 2021, 60, 12175−12188

of SI onto the formation rock.[4] Thus, the injected SI must be compatible with the brine solutions to avoid calcium−inhibitor complex precipitation.

It is crucial to prove whether the potent biodegradable **PAA** SI is compatible with calcium ions and does not form Ca−SI complex precipitation. The calcium compatibility test follows a procedure. Four concentrations of **PAA** of 100, 1000, 10 000, and 50 000 ppm were mixed in 20 mL of distilled water in 20 mL glass jars. Then, various concentrations of Ca^{2+} ions in doses from 10 to 10 000 ppm were mixed with synthetic seawater (3.00% of NaCl) in the corresponding jars. The mixture solutions were adjusted at pH 4−6 to match the reservoir pH. All jars were shaken well until the mixture solution became clear. The appearance of the mixtures was checked at room temperature. The jars were then placed in an oven at 80 °C over the 24 h test period. The compatibility performance (clear, hazy, and precipitate) of **PAA** with calcium ions was checked and recorded by our visual observation after 30 min, 1 h, 4 h, and 24 h.

2.6. Density Functional Theory Simulations. *2.6.1. Molecular Model.* DFT calculations were carried out on the alkali metal complexes with different SIs to reveal the origin of the experimental inhibition performance and establish a structure−function relationship of these inhibitors. We studied two types of SIs, the commercial aminomethylenephosphonate-based SIs (**ATMP** and **DTPMP**) and nitrogen-free phosphonate SIs (**PBTCA**, **HPAA**, **PAA**, and **PPA**). We considered different protonation states of all inhibitors based on their experimental pK_a[1−3] values (Figure 3).[26−28] Geometries were optimized using the wB97xd/def2-SVP level of theory; more accurate energies are obtained at the wB97xd/def2-TZVP level of theory.[29−32] All of the stationary points were verified minimum by frequency calculations and confirmed to have all positive frequencies. The solvent environment was taken into account using the polarizable continuum model (PCM) during the optimization of geometries.[33] Further, we employed the continuum solvation model based on the electronic density of the solute molecule interacting with a continuum solvent (SMD) model developed by Marenich et al., which is recommended by Gaussian 16 to obtain accurate solvation free energies.[34,35]

Metal-binding free energies were calculated based on eq 1.

$$\Delta G_{bind} = G\text{complex} - G[\text{molecule} + \text{metal}] \quad (1)$$

The contribution of the solvation free energy to the total metal-binding free energy was calculated based on eq 2.

$$\Delta G_{solv} = G_{solv}\ \text{complex} - G_{solv}[\text{molecule} + \text{metal}] \quad (2)$$

All binding free energies were corrected for the basis set superposition using the counterpoise method.[36,37] All calculations were performed using Gaussian 16.[35] Since we are interested in the relative binding energies between the different SIs, the vibrational corrections to the total metal-binding free energies are neglected as they are very small compared to the vacuum binding energies and the solvation corrections (it reaches its maximum to 2 kcal/mol). Similarly, the state corrections (1.9 kcal/mol) are neglected.

2.6.2. Solid-State Periodic Model. Solid-state DFT simulations were carried out using the Vienna ab initio simulation package (VASP) with the projector augmented wave (PAW) pseudopotentials and the periodic boundary conditions.[38−40] The Brillouin zone was sampled using a 3 × 3 × 1 Monkhorst-pack γ centered mesh, and Gaussian smearing of 0.02 eV was used for the occupations of the electronic levels. The Perdew−Burke−Ernzerhof (PBE) functional within the generalized gradient approximation (GGA) was used to describe the electron interaction energy of the exchange−correlation.[41,42] The electronic energies were converged within the limit of 10^{-7} eV, and a cutoff of 520 eV was used. All geometries were optimized using 0.03 eV/Å force criteria. van der Waals (VDW) dispersion corrections are adopted using Grimme's D3 scheme. The binding energies of the nitrogen-free SIs were calculated, following eq 1. A slab of 221 supercells is created of a 104 calcite facet and a 001 barite facet, which are reported as the most stable facets of the calcite and barite crystals, respectively.[43] A vacuum of 15 Å is applied along the *Z*-axis to remove the suprious interaction that could occur between the surface and its image due to the periodic boundary condition.

3. RESULTS AND DISCUSSION

3.1. High-Pressure Dynamic Tube-Blocking Test. The inhibition performances of a series of nitrogen-free phosphonate SIs were screened against oilfield scales (calcite and barite) using a high-pressure dynamic tube-blocking rig at 100 °C and 1200 psi. In addition, the inhibition performances of these chemicals were compared to known commercial aminomethylenephosphonate SIs **ATMP** and **DTPMP** to investigate the role of different functional groups onto the inhibitor backbone. The pH of all tested SIs was performed at 4−6 in a 1000 ppm aqueous medium to match the reservoir chemistry conditions. The failed inhibition concentrations (FICs) for all SIs were reported from the first and second inhibitor experiments. Various concentrations of phosphonate-based SIs (1−100 ppm) were pumped over 1 h or until the deposit was determined.

Table 2 summarizes the calcite scale inhibition results for the nitrogen-free phosphonate SIs and two aminomethylene-phosphonate SIs **ATMP** and **DTPMP** for comparative purposes. It was found that both commercial amino-methylenephosphonate SIs gave poor to moderate inhibition performances. The FIC of **ATMP** was 20 ppm after 26 min for the first and repeat tests, while **DTPMP** failed at an FIC of 10

Table 2. FIC Values and Scaling Times for Aminomethylenephosphonate SIs (ATMP and DTPMP) and Nitrogen-Free Phosphonate SIs (PBTCA, HPAA, PAA, and PPA) for Calcite Scale

	calcium carbonate scale					
	first blank	first scale test		second scale test		second blank
scale inhibitor	time (min)	conc. (ppm)	time (min)	conc. (ppm)	time (min)	time (min)
Aminomethylenephosphonate SIs						
ATMP	11	20	26	20	26	12
DTPMP	10	10	20	10	20	12
Nitrogen-Free Phosphonate SIs						
PBTCA	11	1	35	1	30	12
HPAA	9	<1		<1		10
PAA	8	5	25	5	30	8
PPA	9	2	5	2	9	8
PAA[a]	10	2	36	2	32	12

[a]**PAA** was evaluated against the calcium carbonate scale after the thermal heating test (130 °C, 1 week).

https://doi.org/10.1021/acs.iecr.1c02441
Ind. Eng. Chem. Res. 2021, 60, 12175−12188

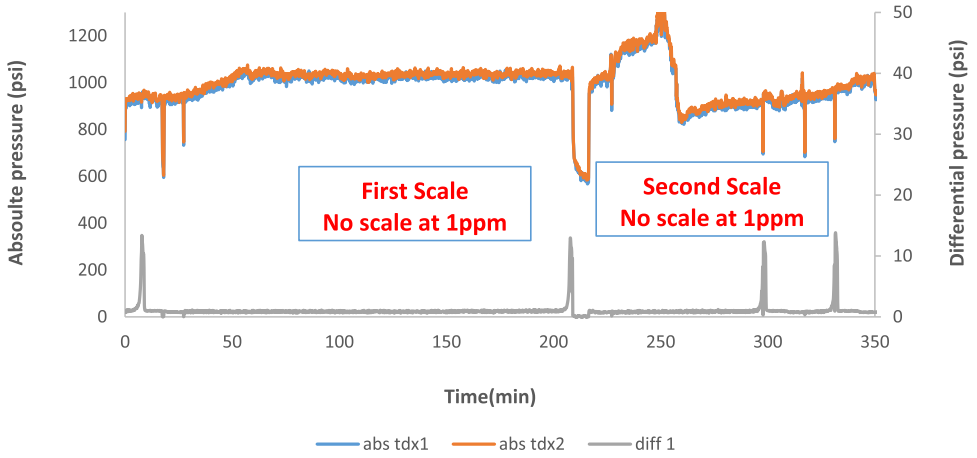

Figure 4. Schematic representation of the calcite scale dynamic scale loop test for **HPAA** SI, showing FIC values and scaling times.

ppm after 20 min. The possible reason for the weak calcite inhibition performances of **ATMP** and **DTPMP** is related to the incompatibility of these SIs with calcium ions, leading to SI−Ca complex precipitation, as explained previously[9,12] and supported by our DFT simulations. Indeed, these molecules display a high capacity to chelate Ca^{2+} ions and form larger aggregates that potentially can be precipitated.

For the nitrogen-free phosphonate SIs, it was found that all of these chemicals gave very good to outstanding calcite inhibition performance in comparison with the known oilfield SIs **ATMP** and **DTPMP**. Among these tested compounds are the chemicals that include only monophosphonic acid and one or several carboxylate groups in their backbone structures. **PBTCA** gave excellent calcite inhibition efficiency with an FIC of 1 ppm after 35 and 30 min for both experiments, respectively. We believe that besides the phosphonate group the presence of several carboxylate groups in **PBTCA** is the origin of its outstanding calcite inhibition performance (see DFT simulations).

Interestingly, **HPAA** exhibited outstanding inhibition performance with no scale observed at 1 ppm for both runs. Figure 4 gives the schematic representation of four stages of **HPAA** in the dynamic tube-blocking rig. The first stage shows that the inorganic deposits were observed after 9 min with no inhibitor where the differential pressure reaches more than 1 bar. This step is also known as the first blank test. Then, the coil was cleaned with the cleaning mixture solution (Na_4EDTA, pH = 11−12) and deionized water, causing the differential pressure to adjust at 1 psi. The dynamic test is started by flushing 5 ppm **HPAA** (second stage). It was found that no deposit was observed at this stage. The test was then conducted by pumping the subsequent programmed SI concentrations of 2 and 1 ppm for 1 h each. It was noted that there was no scale buildup across the coil after 1 h, even at the lowest SI concentration of 1 ppm. Due to no injection of any concentration of **HPAA**, the scale was formed, and then the tubing was cleaned using the same cleaning mixture solution (Na_4EDTA and water). After that, the test was repeated by pumping 2 ppm **HPAA** (third stage). It was noted that the repeat test gave similar results with no scale formed at 1 ppm, affording excellent reproducibility. Finally, the test was finished with another blank experiment with no **HPAA** SI (fourth stage). The scale was rapidly formed after 10 min.

This class of SI contains monophosphonate and mono-carboxylate groups and one hydroxyl group. This superior performance may be associated with the extra hydroxyl group on the SI structure chain, which improves the metal-binding abilities of the SI to calcite crystal surfaces. We have recently reported that bisphosphonate (BP) SI-bearing hydroxyl groups provided better carbonate inhibition efficiency than the BP−SI-containing amino moieties.[17]

Naturally occurring **PAA** also showed very good inhibition performance for oilfield calcite scaling. The FIC of **PAA** was 5 ppm after 25 and 30 min for both experiments, as tabulated in Table 2. Another class of simple nitrogen-free phosphonates containing the monocarboxylate moiety is **PPA. PPA** is related to biodegradable **PAA** SI by virtue of having one more carbon in the chain structure. **PPA** exhibited excellent inhibition efficiency with an FIC of 2 ppm after 5 and 9 min for both experiments, respectively (Table 2). We suggest that the distance between the phosphonate moiety and the carboxylate moiety impacts the inhibition activity.

Table 3 summarizes the FIC values and scaling times for aminomethylenephosphonate SIs (**ATMP** and **DTPMP**) and nitrogen-free phosphonate SIs (**PBTCA**, **HPAA**, **PAA**, and **PPA**) for the barite scale. Two commercially **ATMP** and **DTPMP** SIs gave reasonable barite scale inhibition perform-

Table 3. FIC Values and Scaling Times for Aminomethylenephosphonate SIs (ATMP and DTPMP) and Nitrogen-Free Phosphonate SIs (PBTCA, HPAA, PAA, and PPA) for the Barite Scale

	barium sulfate scale					
	first blank	first scale test		second scale test		second blank
scale inhibitor	time (min)	conc. (ppm)	time (min)	conc. (ppm)	time (min)	time (min)
Aminomethylenephosphonate SIs						
ATMP	11	10	42	10	41	11
DTPMP	10	5	5	5	9	10
Nitrogen-Free Phosphonate SIs						
PBTCA	7	50	14	50	14	8
HPAA	8	20	15	20	20	9
PAA	7	100	25	100	25	9
PPA	7	100	15	100	14	8
PAA[a]	7	100	11	100	12	7

[a]**PAA** was evaluated against the sulfate scale after the thermal heating test (130 °C, 1 week).

https://doi.org/10.1021/acs.iecr.1c02441
Ind. Eng. Chem. Res. 2021, 60, 12175−12188

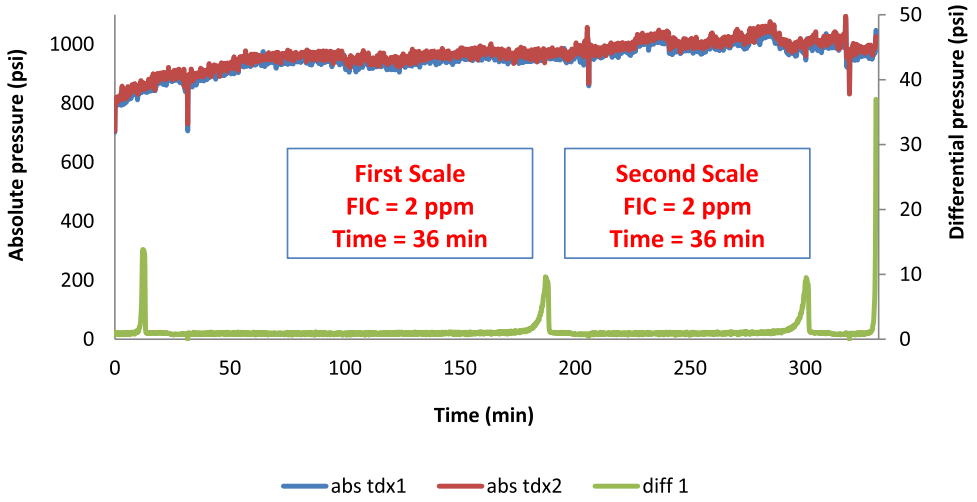

Figure 5. Schematic representation of the calcite scale dynamic scale loop test (FIC vs time) for **PAA** after thermal aging at 130 °C.

ance. For example, **ATMP** failed at 10 ppm, and **DTPMP** gave an FIC of 5 ppm for both runs. It is well-known that the SI incorporating several phosphonate groups enhances the surface-active properties of phosphonate-based SIs, leading to a powerful binding affinity of the molecule with barite scaling.[44]

For the nitrogen-free phosphonate SIs, we speculated that all of these chemicals gave a poor barite inhibition performance because of the few numbers of phosphonate groups in their backbone structures. As stated earlier and investigated in our previous reports, the number of phosphonate groups in the inhibitor structure backbone plays a vital inhibition role against the barite scaling in the upstream oil and gas industry.[7,12]

PBTCA gave a moderate barite scale inhibition with an FIC of 50 ppm after 14 for both runs (Table 3). **HPAA** gave the best barite inhibition efficiency performance in comparison with the other nitrogen-free phosphonate SIs. The FIC of **HPPA** was 20 ppm after 15 and 20 min for both runs, respectively. We have recently investigated that the hydroxyl moiety enhances the binding activity of the phosphonated SIs.[17]

Furthermore, **PAA** and **PPA** gave the weakest inhibition performances for the barite scaling. The FICs of **PAA** indicated rapid scaling after 15 min in the first run and 14 min in the repeated test at 100 ppm, as presented in Table 3. In addition, **PPA** also failed at 100 ppm.

Based on the above scale inhibition performance results, it was investigated that all tested nitrogen-free phosphonate SIs gave powerful calcite inhibition efficiency performances compared to known commercial aminomethylenephosphonate SIs. Moreover, nitrogen-free monophosphonate SIs bearing hydroxyl and carboxylate groups exhibited better oilfield calcite inhibition performance compared to nitrogen-free monophosphonate SIs containing only the carboxylate group. This highlights the crucial binding role of the hydroxyl group in inhibiting calcite scales.

3.2. Thermal Stability Test. Several attempts have been reported to develop biodegradable phosphonated SIs at HPHT conditions in the upstream oil and gas industry.[4,12−18] Thus, there is a clear need to explore more environmentally friendly phosphonate-based SIs for squeeze treatment applications to enhance SI retention onto the formation rock, affording prolonged oilfield scale inhibition lifetimes. A 5 wt % mixture solution of naturally occurring **PAA** was aged at 130 °C for 7 days under nitrogen gas (anaerobic conditions). The aged **PAA** was then retested against calcite and barite scales in the dynamic scale loop test at 100 °C and 80 bar. The FICs and scaling times of aged inhibitors for calcite and barite scales are summarized in Tables 2 and 3.

Interestingly, the aged **PAA** improved the inhibition performance for calcite scaling compared to the unaged sample under the same test conditions. The FIC of the aged **PAA** was 2 ppm after 36 min in the first round and 32 min in the second round, as shown in Figure 5. This means that **PAA** is thermally stable for the calcite scale at HPHT oilfield conditions and can be proposed as a potential candidate for oilfield scale squeeze treatment applications. We are currently trying to explain this inhibition improvement of aged **PAA** using various spectroscopic techniques. It was also found that the aged **PAA** gave the same inhibition performance results of the unaged sample for the barite scale, providing an FIC at 100 ppm after 11 and 12 min for both rounds, respectively.

3.3. OECD 306 Seawater Biodegradation Test. Table 4 summarizes seawater biodegradation activities of all tested SIs

Table 4. Biodegradability Activity Measured by the OECD

SIs	% BOD28 by OECD 306
seawater	0
sodium benzoate	90
DTPMP	15[12]
ATMP	34[12]
PBTCA	37
HPAA	28
PAA	>80[46]
PPA	32

using the in-house OECD 306 test procedure. This protocol was carried out by the closed bottle method over 28 days. In addition, all experiments were tested in triplicate, and the final biological oxygen demand (BOD) percentage is given here (Table 4) according to the average values of triplet experiments.

The biodegradable standard reference sodium benzoate afforded an excellent BOD28 value of 90%. Commercial aminomethylenephosphonate SIs gave a poor BOD28 performance of 15% for **DTPMP** and moderate BOD28

https://doi.org/10.1021/acs.iecr.1c02441
Ind. Eng. Chem. Res. 2021, 60, 12175−12188

activities of 34% for **ATMP**, as described previously.[12] It was reported that the carboxyl group in the SI backbone structure is clearly advantageous for improving the biodegradability properties. For example, polycarboxylic acid SI afforded an excellent BOD28 value of >60% over 28 days using the OECD 306 seawater biodegradation test. Polycarboxylic acid has been deployed as a green SI in the North Sea.[15,45] All of the tested nitrogen-free phosphonate SIs in this project contain a carboxylate group. Therefore, we believe that all of these chemicals will afford a reasonable biodegradation efficiency performance. **PBTCA** exhibited moderate biodegradation activity of 37% over 28 days, as shown in Table 4. In addition, **HPAA** also showed a moderate biodegradation rate of 28% in 28 days. We previously found that the hydroxyl group in the inhibitor backbone structure led to poor biodegradation activities. The stability of **HPAA** might be due to the strong hydrogen bond between the carboxylate and hydroxyl groups.[15] Furthermore, **PPA** afforded a reasonable BOD28 value of 32% (Table 4).

In general, these classes of chemicals can be proposed as environmentally friendly oilfield SIs in regions with strict environmental regulations, according to the Oslo and Paris Commission (OSPARCOM) for oilfield chemicals. It has been stated that the chemicals indicating 20−60% biodegradation activities based on the OECD 306 protocol are categorized as Gold with no restrictions in the offshore United Kingdom and Yellow-2 with further evaluations in offshore Norway.

Interestingly, Fisher et al. reported that **PAA** gave a superior BOD rate of >80% over 28 days using the approved marine OECD 306 protocol.[46] According to the OSPAR Convention, **PAA** can be categorized as Yellow 1 with no restrictions for use in offshore Norway. Moreover, **PAA** is a naturally occurring product and drug compound, and it can be listed in the Poses Little Or No Risk (PLONOR to the Environment) database. Furthermore, the biodegradation activities are significantly increased from **PPA** (alkane = ethane) to **PAA** (alkane = methane) by just decreasing the number of carbon atoms in the structure backbone between the carboxylate and phosphonate groups. This highlights the sensitive nature of seawater bacteria to admit and degrade organic compounds.

3.4. Calcium Compatibility Test. The outstanding results from biodegradation, thermal stability, and calcite scale dynamic scale loop tests of the **PAA** encouraged us to study its compatibility performance with calcium ions. It is very important to monitor the calcium tolerance for the SIs with high calcium brines in the petroleum reservoir, particularly for squeeze treatment applications. It is commonly known that various phosphonate-based SIs are intolerant to calcium ions, causing Ca^{2+}−SI complex precipitation. This calcium intolerance problem can lead to formation damage and poor placement of the inhibitor onto the formation rock during the squeeze treatment process.

We decided to study the calcium tolerance performance of the highly biodegradable SI **PAA** at various SI and Ca^{2+} ion concentrations. The concentrations of SI were in the range of 100−50 000 ppm, and the Ca^{2+} ion concentrations changed from 100 to 10 000 ppm. The test was operated at 80 °C in the presence of 30 000 ppm sodium chloride. The obtained results showed that all concentrations of **PAA** (up to 50 000 ppm) gave excellent calcium tolerance efficiency performances with all Ca^{2+} concentrations (up to 10 000 ppm) throughout the test period. Interestingly, no haziness or precipitation was observed throughout the test period. Table 5 summarizes the most extreme matrix of **PAA** (100−50 000 ppm) at 10 000 ppm calcium ions. We assume that the carboxylate group improved the chelation properties of **PAA** with Ca^{2+} ions.

Table 5. Compatibility Activity of PAA at 10 000 ppm Ca^{2+} Ions and 30 000 ppm NaCl

	appearance				
SI (ppm)	at mixing	30 min	1 h	4 h	24 h
100	clear	clear	clear	clear	clear
1000	clear	clear	clear	clear	clear
10 000	clear	clear	clear	clear	clear
50 000	clear	clear	clear	clear	clear

3.5. Quantum Chemical Studies. DFT simulations were carried out using molecular and solid-state models to gain insights into the inhibition mechanism of the considered SIs with our focus on the nitrogen-free structures. The molecular models are designed to examine the cation-compatibility of these SIs. Therefore, the affinity of the inhibitor molecules toward the common cations existing in the reservoir brines (i.e., Ca^{2+}, Mg^{2+}, Ba^{2+}, and Na^{+}) has been calculated. We have considered different protonation states of the SIs based on their experimental pK_a and two pH values (6 and 10).[26−28] It is essential to highlight that when we calculated the metal solvation free energies, we found that the SMD model does not reproduce the experimental values of metal solvation energies as the model was parameterized for the organic molecules. Consequently, to obtain reliable metal-binding free energies, we optimized the atomic radii in the continuum solvent model (SMD) to minimize the difference between the calculated and experimental solvation free energies (see Table S1). Then, we used the optimized metal parameters to calculate the solvation free energies of the metal complexes, which are required to calculate the metal-binding free energies. For example, an approach was successfully applied for the stability constant calculations of mercury complexes.[47]

3.5.1. Affinity of the Aminomethylenephosphonate-Based SIs. First, we investigated the affinity of two common commercial aminomethylenephosphonate-based SIs with different cations in the reservoir brines (i.e., Ca^{2+}, Mg^{2+}, Ba^{2+}, and Na^{+}). The results reported in Tables 6 and S2 indicate a high affinity of these molecules toward all of the metal cations, especially the divalent. The nitrogen-based SIs show a strong capacity to bind the different cations in the brine, which indicates a low tolerance of these molecules toward these ions. Also, the affinity of the nitrogen-based SIs is superior at high pH for Ca^{2+} and Mg^{2+} ions, while we observed the inverse trend for Ba^{2+} and Na^{+} ions. The origin of the trend is the different ionic charge densities of these cations. The ionic sizes of Ba^{2+} and Na^{+} make them carry less charge densities than Ca^{2+} and Mg^{2+}, which consequently influences their electrostatic interactions with the SI molecules. Therefore, Ba^{2+} and Na^{+} display their maximum affinities at low pH because at these conditions, SI molecules carry less charge (protonated at some sites), which attenuates the electrostatic repulsion in the cation's coordination shell (Tables 6 and S2). The affinity of **DTPMP** is significantly higher than that of **ATMP** for both Ca^{2+} and Ba^{2+} ions, which indicates that these molecules bind very well to the surface of both calcite and barite. The strong binding energies of the metal cations with **DTPMP** over **ATMP** demonstrate the importance of the number of phosphonate and aminomethylene groups for the SIs' affinity toward the different minerals. However, the barium sulfate

https://doi.org/10.1021/acs.iecr.1c02441
Ind. Eng. Chem. Res. 2021, 60, 12175−12188

Table 6. Binding Free Energies of DTPMP and ATMP Inhibitors to Ca^{2+} and Ba^{2+} (Parenthesis) Ions (Reported in kcal/mol)

SIs	ΔE_{gas}	$\Delta E_{Sol.}$	$\Delta E_{Total.}$
$DTPMPH_4$	−1122.18 (−1057.79)	1046.33 (981.98)	−75.85 (−75.81)
$DTPMPH_2$	−1408.85 (−1332.11)	1321.56 (1254.08)	−87.28 (−78.03)
DTPMP	−1659.32 (−1545.62)	1565.98 (1471.66)	−93.34 (−73.96)
$ATMPH_2$	−874.84 (−820.40)	818.31 (762.27)	−53.53 (−58.13)
ATMPH	−1024.66 (−976.58)	967.97 (918.34)	−56.69 (−58.24)
ATMP	−1174.65 (−1080.28)	1114.74 (1028.80)	−59.91 (−51.48)

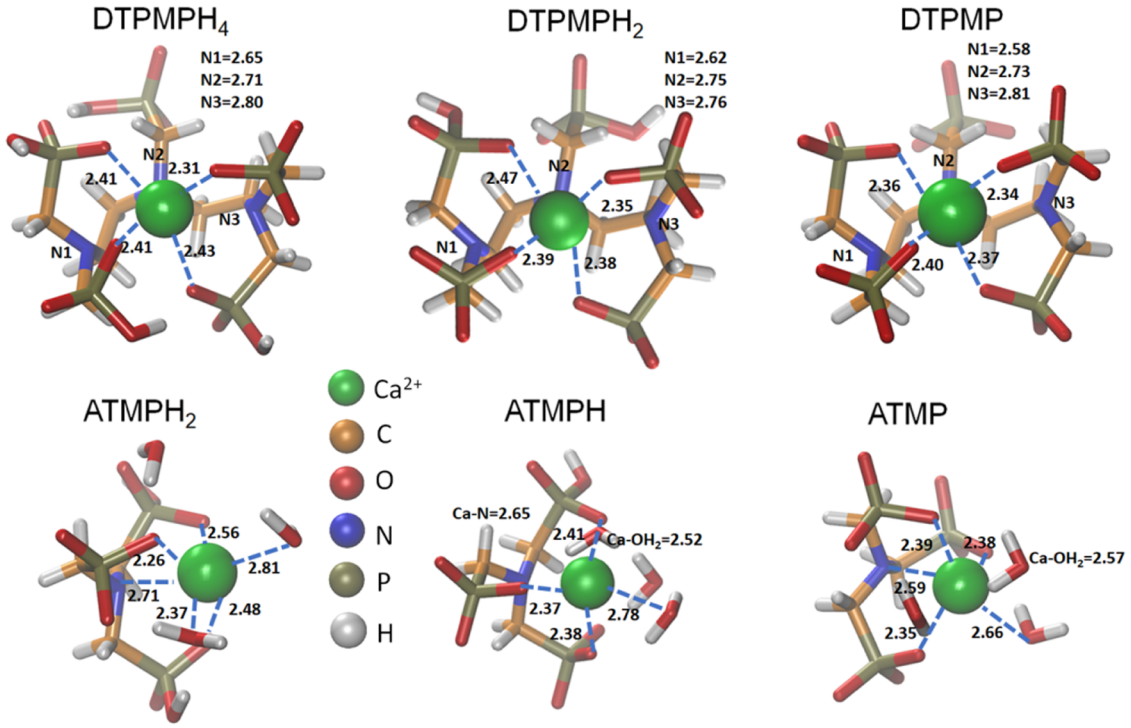

Figure 6. Optimized structures of the metal−SI complexes for Ca^{2+} for the commercial aminomethylenephosphonate-based inhibitors are shown in sticks, and Ca^{2+} ions are in spheres. Coordination distances are reported in angstrom.

scale inhibition is relatively more efficient than the calcium carbonate scale using **DTPMP** and **ATMP**. The performance difference of the considered SIs can be explained by the formation kinetics of the two scales' formation. Indeed, Jones et al. reported that the formation of the barium sulfate crystals proceeds via the formation of amorphous aggregates, which are more stable than the crystalline ones. The crystal growth occurs through the restructuring of these amorphous aggregates. The authors claimed that this step could be rate-limiting for crystal formation.[48] However, calcium carbonate crystals do not follow the exact mechanism proposed by Spanos et al.[49] The sluggish kinetics of barium sulfate crystals compared to calcium carbonate can be the origin of the efficiency of **ATMP** and **DTPMP** for the barium scale inhibition. Such a delay in crystal formation gives enough time for the SIs to interact with the different facets of the amorphous and crystalline particles to prevent crystal growth and hence inhibit scale formation.

Regarding the structure of the metal−SI complex, the chelating mode of these compounds is reserved among all of the cations (Figures 6, S2, and S3). Focusing on the Ca^{2+} complexes, in **DTPMP**, it is coordinated by seven bonds, four of them with the phosphonate groups (with an average Ca−O distance of 2.39 Å) and three from the nitrogen atoms of the molecule backbone (with an average Ca−N distance of 2.71 Å; Figure 6). The fifth phosphonate group cannot penetrate the Ca^{2+} coordination shell due to the strong electrostatic repulsion. In the Ca^{2+}−**ATMP** complexes, calcium has six coordination bonds, three of the phosphonates (with an average Ca−O distance of 2.39 Å), one nitrogen atom (with an average Ca−N distance of 2.65 Å), and two water molecules (with an average Ca−OH_2 distance of 2.64 Å). Although the strong electrostatic interaction between the chelating phosphonate groups and cations enhanced the formation of the complexes, the dehydration of both inhibitors and cations is the main hurdle against the formation of the cation−SI complexes (Tables 6 and S2). The ionic size of the considered cations plays an important role, reflected in the cationic charge density. The affinities of SI molecules toward Mg^{2+} are higher than the rest of the cations. Mg^{2+} has a smaller size, which leads to a higher charge density that makes the electrostatic interaction with the negatively charged groups become significantly strong (Table 6). The same trend is valid when we compare Ca^{2+}, Ba^{2+}, and Na^{+}. Herein, we did not observe the decisive role of the metal dehydration free energy because the dehydration of the SI molecules is dominant and reaches up to 9.0 times the metal dehydration free energy as in the case of Ca^{2+}−**DTPMP** (Tables S3 and S4). The coordination of the different metals with the aminomethylenephosphonate is also correlated with the ionic size; the shortest M−O and M−N

https://doi.org/10.1021/acs.iecr.1c02441
Ind. Eng. Chem. Res. 2021, 60, 12175−12188

bonds are observed for Mg^{2+} complexes (Figure S1), and the longest was observed for Ba^{2+} complexes (Figure S2). The electron transfer from the SIs into the metal cation is also an important parameter and is correlated to the strength of the metal-binding energies. Indeed, in the case of the Mg^{2+}−**DTPMP** complex, there is 1.13 *e*, which is transferred from **DTPMP** into Mg^{2+} against 0.87 *e* for Ca^{2+}, 0.79 *e* for Ba^{2+}, and 0.11 *e* for Na^{+}.

We further optimized two **DTPMP** molecules with three calcium ions to examine the possibility of explaining the calcium tolerance of the aminomethylenephosphonate-based inhibitors at high concentrations. The optimized structure of the 2**DTPMP**:3Ca^{2+} complex is shown in Figure 7; the

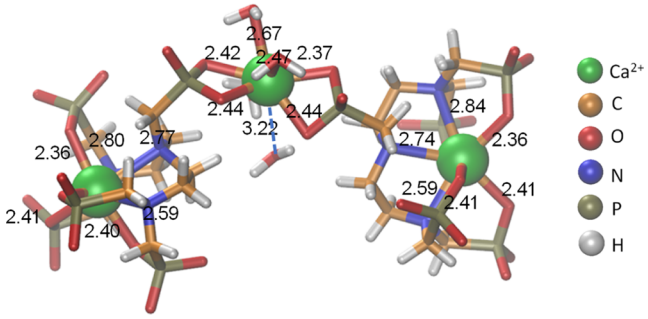

Figure 7. Optimized structures of two molecules of **DTPMP** chelating three calcium ions. **DTPMP** is shown in sticks, and Ca^{2+} ions are in green spheres.

extended phosphonate group of **DTPMP** can interact with more calcium ions and make larger aggregates of **DTPMP**:Ca^{2+}, which can be precipitated at higher calcium concentrations. The calculated affinity of the bridged calcium site was found to be −66.67 kcal/mol favorable but less than the primary binding site of **DTPMP** (Table 6). This result indicates that this site can be easily populated at high concentrations and can lead to precipitation of **DTPMP**:Ca^{2+}. Such a low calcium tolerance of the commercial SIs also affects their scale inhibition capacity; the strong interaction with the free cations in the solution brine leads to minimizing the amount of SIs adsorbed on the mineral surfaces and increases the amount of inhibitor to reach the required surface coverage for scale inhibition.

3.5.2. Affinity of the Nitrogen-Free Phosphonate-Based SIs. Similarly, we have calculated the binding free energies of the reservoir cations (i.e., Ca^{2+}, Mg^{2+}, Ba^{2+}, and Na^{+}) toward four potential inhibitors of nitrogen-free phosphonate structures (**PBTCA**, **HPAA**, **PAA**, and **PPA**) to examine their application as antiscaling agents in the oilfield industry with a focus on their ionic tolerance, especially Ca^{2+}. Results reported in Tables 7 and S5 indicate that the nitrogen-free phosphonate molecules are very good scale inhibitors compared to these commercial SIs. Indeed, they have much less affinity toward the free cations, especially the divalent cations (Ca^{2+} and Ba^{2+}), which are the primary sources of scale formations, as shown in Figure 8. The nitrogen-free inhibitors display good affinities over a wide range of pH without a significant activity difference. Experimentally, nitrogen-free SIs are much better inhibitors for calcium carbonate than nitrogen-based SIs. The nitrogen-free SIs display FIC in the range of 1−5 ppm, while the nitrogen-based ones exhibit higher FIC over 10 ppm. The calcium tolerance of the nitrogen-based ones can explain this performance trend. **DTPMP** and **ATMP** molecules are bulky and have multiple negatively charged groups, especially **DTPMP**, that can be precipitated in the presence of Ca^{2+} ions, as mentioned above. In addition, the diffusion of small molecules as the nitrogen-free SIs is much faster than the bulky aminomethylenephosphonate-based inhibitors. This led to more rapid binding kinetics of the nitrogen-free SIs on the mineral surfaces than the commercial SIs.

Further, the metal coordination of the nitrogen-free phosphonate SIs is partially solvated, which makes their diffusion easier and improves their calcium tolerance. Similarly, the shortest M−O is observed for Mg^{2+} complexes and the longest for Ba^{2+} complexes. The same trend of the chelating pattern for aminomethylenephosphonate-based inhibitors is observed for the nitrogen-free SIs.

3.5.3. Adsorption of N-Free Molecules on Calcite and Barite Surfaces. The periodic DFT simulations were adopted to examine the adsorption strength of the nitrogen-free molecules on the most stable facets of the two minerals of the scales (i.e., calcite 104 and barite 001). To minimize the computational cost, we used three layers of the mineral. The bottom two layers are fixed, and the top layer is allowed to relax during the geometric optimization of the SIs on their surfaces. Experimentally, the N-free molecules efficiently inhibit the calcite scale much more than the barite one. At this concentration regime, the primary inhibition mechanism prevents crystal growth via the adsorption of scale inhibitors on the different facets of the scaling mineral. Results reported in Table 8 indicate favorable interactions between the nitrogen-free SIs and the two considered facets of calcite and barite. However, the affinities of the nitrogen-free SIs for calcite surfaces are much stronger than for the barite scale, which correlates well with the inhibition trend for the two scales. **PBTCA** is found to be the most stable binder on the two mineral facets. No significant binding differences are observed for the remaining N-free inhibitors because the structural

Table 7. Binding Free Energies of Nitrogen-Free Phosphonate SI Inhibitors (PBTCA, HPAA, PAA, and PPA) to Ca^{2+} and Ba^{2+} (Parenthesis) Ions (Reported in kcal/mol)

SIs	ΔE_{gas}	$\Delta E_{Sol.}$	$\Delta E_{Total.}$
PBTCA	−993.33 (−907.56)	941.90 (864.80)	−51.43 (−42.76)
PBTCAH	−849.93 (−785.51)	800.28 (733.70)	−49.65 (−51.81)
HPAA	−750.38 (−848.39)	702.82 (789.55)	−47.56 (−46.02)
HPAAH	−587.90 (−502.23)	534.20 (458.90)	−44.71 (−43.33)
PAA	−719.40 (−668.74)	676.28 (621.53)	−43.12 (−47.21)
PAAH	−566.21 (−542.91)	480.76 (494.39)	−41.09 (−48.52)
PPA	−744.77 (−658.96)	696.26 (611.52)	−48.51 (−47.44)
PPAH	−586.20 (−491.94)	540.38 (452.16)	−45.82 (−39.78)

https://doi.org/10.1021/acs.iecr.1c02441
Ind. Eng. Chem. Res. 2021, 60, 12175−12188

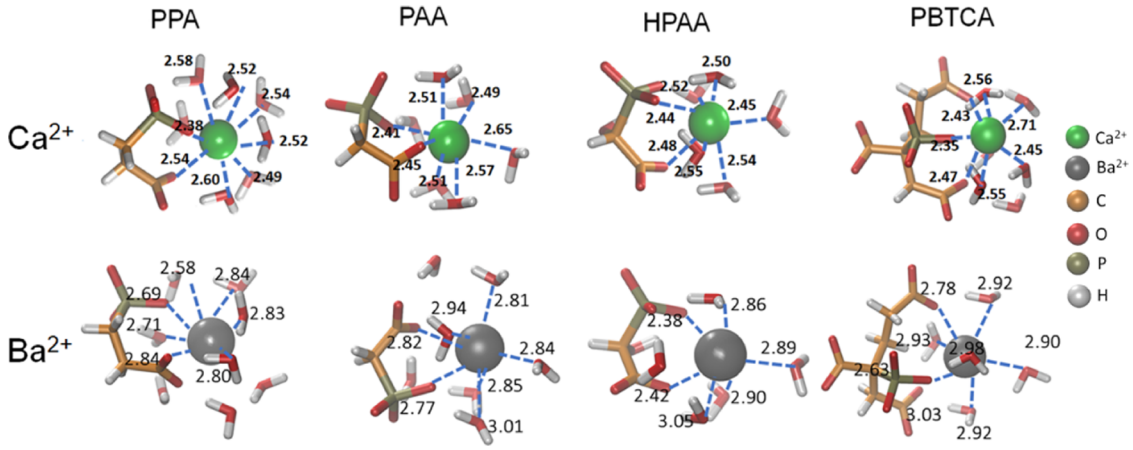

Figure 8. Optimized structures of the metal−SI complexes for Ca^{2+} (green) and Ba^{2+} (gray) with nitrogen-free phosphonate-based inhibitors shown in sticks and cations in spheres. Coordination distances are reported in angstrom.

Table 8. Adsorption Energies of Nitrogen-Free Phosphonate SI Inhibitors on Calcite 104 and Barite 001 Surfaces (PBTCA, HPAA, PAA, and PPA) (Reported in Electronvolt)

SIs	calcite	barite
PBTCA	−11.73	−7.44
HPAA	−3.52	−1.40
PAA	−3.70	−1.64
PPA	−3.82	−3.01

differences are very subtle among **PAA**, **HPAA**, and **PPA** molecules.

The stronger interactions between the SIs on the calcite 104 facet are mainly due to the electrostatic repulsion between the sulfate anion and the inhibitors. The tetrahedral geometry of sulfate makes it more solvent-exposed than the linear carbonate anion. Consequently, it induces higher electrostatic repulsion with the inhibitor's oxygen atoms than carbonate. This is evidenced in the metal−oxygen distances observed for the inhibitors on the two facets. In the case of calcite−SI complexes, the metal−oxygen distances are shorter than for barite−SI complexes (Figure 9). The higher affinities with the calcite surface explain well the experimental trend of FIC values of the nitrogen-free molecules compared to the barite scale. As we previously mentioned, the kinetics of the barite scale formation is sluggish and involves the formation of amorphous and crystalline aggregates. The nature of these aggregates makes the inhibition mechanism complex and challenging to interpret. These amorphous aggregates undergo restructuring into crystalline ones in a slow kinetic process.[48] Thus, the potential energy surface of the barite scale formation is complicated, and we cannot sample all of the states. Such a complex potential energy surface enriches the potential adsorption sites that require a higher amount of the inhibitor to reach the required coverage for the barite scale inhibition. Previous reports showed that only 3−5% of the surface coverage is required for efficient calcite scale inhibition.[50]

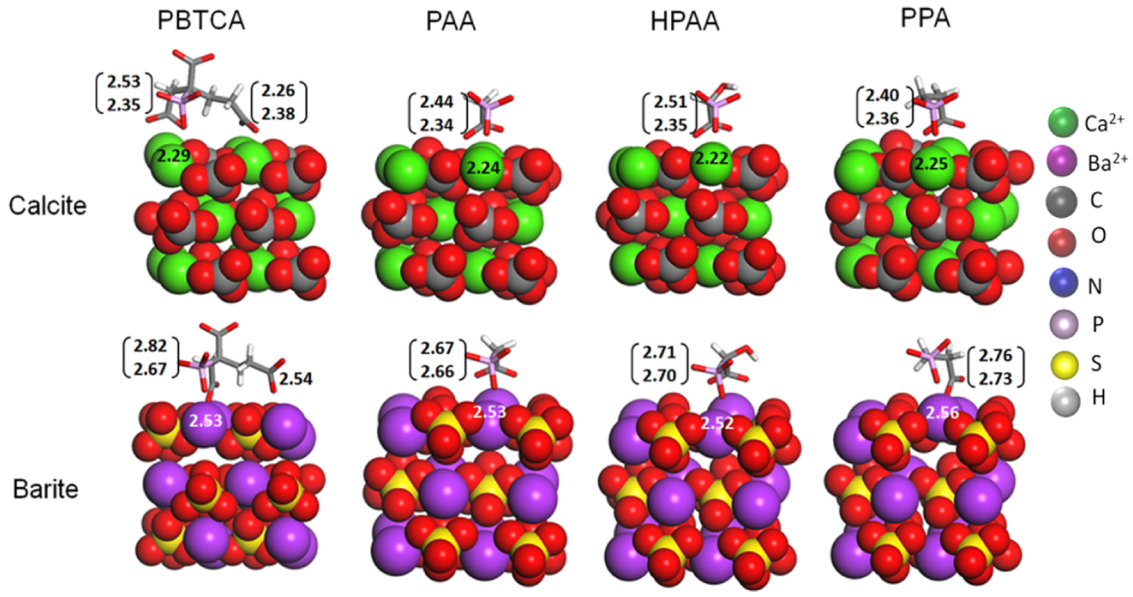

Figure 9. Optimized structures of the nitrogen-free phosphonate-based inhibitors adsorbed on calcite 104 and barite 001 facets. The bond distance of metal−oxygen is reported in angstrom, and the bidentate carboxylate−metal distances are reported in parenthesis. Color code: Ca^{2+}, green; Ba^{2+}, magenta; O, red; S, yellow; C, dark brown; P, thistle; and H, white.

https://doi.org/10.1021/acs.iecr.1c02441
Ind. Eng. Chem. Res. 2021, 60, 12175−12188

However, this percentage increases to 16% for barite, which agrees well with our hypothesis mentioned above.[51]

4. ECOLOGICAL TOXICITY PREDICTIONS

The ecological toxicity properties of the studied N-free SIs were studied using AdmetSAR software to examine whether they can be considered as environment-friendly inhibitors.[52] The predicted properties are reported in Table S8. All inhibitors are predicted to be safe against carcinogenicity, ames mutagenesis, and crustacean aquatic toxicities. Interestingly, AdmetSAR predicted that all inhibitors are biodegradable, with the highest probability recorded for the **PAA** molecule. Concerning aquatic fish toxicity, **PAA** and **PPA** are predicted to be safe, while **PBTCA** and **HPAA** are considered to be highly toxic. This suggests that **PAA** and **PPA** can be applied in production operations in offshore fields. The predicted solubility varies from soluble to very soluble (**PBTCA**) due to several hydrogen-bond acceptors and donors that exist in these molecules. All inhibitors are toxic for acute oral, honeybee, and eye irritation toxicities.

5. CONCLUSIONS

As a continuation of our Green Production Chemicals Program to explore new biodegradable, thermally stable, and high-calcium-tolerance oilfield scale inhibitors bearing a phosphonic acid moiety, a series of nitrogen-free phosphonates (**BTCA**, **HPAA**, **PAA**, and **PPA**) were evaluated using various tests, including a high-pressure dynamic tube-blocking inhibition efficiency method, thermal aging, calcium tolerance, and seawater biodegradability. Our results showed that all tested nitrogen-free phosphonates gave very good to excellent inhibition performance against the calcite scale at 100 °C and 80 bar compared to both commercial SIs **ATMP** and **DTPMP**. For example, **HPAA** exhibited outstanding inhibition performance with no scale observed at 1 ppm for both runs. Also, naturally occurring **PAA** showed very good inhibition performance for calcite scaling. The FIC of **PAA** was 5 ppm after 25 and 30 min for both experiments. Interestingly, the superior biodegradable SI **PAA** (BOD28 > 80%)[46] displayed excellent thermal stability properties, affording a better scale inhibition efficiency when aged for 7 days at 130 °C. Moreover, **PAA** showed outstanding calcium compatibility activities at all calcium ion (up to 10 000 ppm) and SI (up to 50 000 ppm) concentrations. It was also found that all tested nitrogen-free phosphonates in this project gave moderate inhibition performance for barite scaling. DFT simulations predicted that **DTPMP** and **ATMP** displayed higher affinities for the free cations compared to the nitrogen-free SIs, which explain their calcium compatibilities. The tested nitrogen-free molecules exhibit more calcium tolerance, and they show very good competitiveness compared to commercial inhibitors regarding calcium tolerance. Further, the solid-state DFT simulations predicted a favorable interaction of the nitrogen-free molecules with the surfaces of calcite and barite. However, they have superior affinities toward calcite than with barite, which is in very good agreement with the experimental FIC values. The sluggish kinetics of the barite scale formation could explain the high FIC of the nitrogen-free molecules. The barite crystal growth occurs through the restructuring of preceding amorphous aggregates as reported by Jones et al.[48] Such aggregates enrich the potential adsorption sites for the nitrogen-free SIs and increase the amount of inhibitor necessary to reach the required surface coverage for the barite scale inhibition. In summary, our antiscaling experimental evaluation and the DFT simulations indicate that the nitrogen-free molecules show good potential as calcite scale inhibitors. However, these molecules require further optimization to improve their performance against the barite scale. AdmetSAR predictions support the high biodegradability of the N-free inhibitors and their safety against many environmental issues.

■ ASSOCIATED CONTENT

Supporting Information

The Supporting Information is available free of charge at https://pubs.acs.org/doi/10.1021/acs.iecr.1c02441.

Figure of the dynamic tube-blocking rig, figures of the optimized structures of Mg^{2+} and Na^{+} with the nitrogen-based and nitrogen-free antiscaling agents, metal solvation free energies with the optimized SMD parameters, Mg^{2+} and Na^{+} binding free energies with **DTPMP** and **ATMP**, solvation free energies of the metal complexes and the SIs, and Mulliken atomic charges of the metal−SI complexes for the deprotonated N-free and commercial SIs (PDF)

■ AUTHOR INFORMATION

Corresponding Author

Mohamed F. Mady − *Department of Chemistry, Bioscience and Environmental Engineering, Faculty of Science and Technology, University of Stavanger, N-4036 Stavanger, Norway; Department of Green Chemistry, National Research Centre, Cairo 12622, Egypt;* orcid.org/0000-0002-4636-0066; Email: mohamed.mady@uis.no

Authors

Safwat Abdel-Azeim − *Center of Integrative Petroleum Research (CIPR), College of Petroleum and Geosciences (CPG), King Fahd University of Petroleum and Minerals, Dhahran 31261, Saudi Arabia;* orcid.org/0000-0001-8611-1251

Malcolm A. Kelland − *Department of Chemistry, Bioscience and Environmental Engineering, Faculty of Science and Technology, University of Stavanger, N-4036 Stavanger, Norway;* orcid.org/0000-0003-2295-5804

Complete contact information is available at: https://pubs.acs.org/10.1021/acs.iecr.1c02441

Notes

The authors declare no competing financial interest.

■ ACKNOWLEDGMENTS

S.A.-A. thanks King Abdullah University of Science & Technology (KAUST) in Thuwal, Saudi Arabia, for allowing the use of computational resources of the supercomputer Shaheen.

■ REFERENCES

(1) Rueff, J.-M.; Hix, G. B.; Jaffrès, P.-A. Rigid Phosphonic Acids as Building Blocks for Crystalline Hybrid Materials. In *Tailored Organic−Inorganic Materials*; Brunet, E.; Colón, J. L.; Clearfield, A., Eds.; John Wiley & Sons, Inc., 2015; pp 341−393.

(2) Queffélec, C.; Petit, M.; Janvier, P.; Knight, D. A.; Bujoli, B. Surface Modification Using Phosphonic Acids and Esters. *Chem. Rev.* **2012**, *112*, 3777−3807.

(3) Heymann, D. Bisphosphonates and bone diseases: past, present and future. *Curr. Pharm. Des.* **2010**, *16*, 2948−2949.
(4) Kelland, M. A. *Production Chemicals for the Oil and Gas Industry*, 2nd ed.; CRC Press (Taylor & Francis Group): Boca Raton, FL, 2014.
(5) Sallis, J. D.; Juckes, W.; Anderson, M. E. Phosphocitrate Potential to Influence Deposition of Scaling Salts and Corrosion. *Mineral Scale Formation and Inhibition*; Springer, 1995; Vol. *54*, pp 87−98.
(6) Brandeis, G.; Jaupart, C. The kinetics of nucleation and crystal growth and scaling laws for magmatic crystallization. *Contrib. Mineral. Petrol.* **1987**, *96*, 24−34.
(7) Guo, J.; Severtson, S. Inhibition of Calcium Carbonate Nucleation with Aminophosphonates at High Temperature, pH and Ionic Strength. *Ind. Eng. Chem. Res.* **2004**, *43*, 5411−5417.
(8) Jordan, M. M.; Mackay, E. J.; Vazquez, O. *The Influence of Overflush Fluid Type on Scale Squeeze Life Time-Field Examples and Placement Simulation Evaluation*, CORROSION 2008; NACE International Corrosion, Paper No. NACE-08356; NACE International, 2008.
(9) Mady, M. F.; Kelland, M. A. Overview of the synthesis of salts of organophosphonic acids and their application to the management of oilfield scale. *Energy Fuels* **2017**, *31*, 4603−4615.
(10) Moedritzer, K.; Irani, R. R. The Direct Synthesis of α-Aminomethylphosphonic Acids. Mannich-Type Reactions with Orthophosphorous Acid. *J. Org. Chem.* **1966**, *31*, 1603−1607.
(11) Dyer, S. J.; Anderson, C. E.; Graham, G. M. Thermal stability of amine methyl phosphonate scale inhibitors. *J. Pet. Sci. Eng.* **2004**, *43*, 259−270.
(12) Mady, M. F.; Bagi, A.; Kelland, M. A. Synthesis and Evaluation of New Bisphosphonates as Inhibitors for Oilfield Carbonate and Sulfate Scale Control. *Energy Fuels* **2016**, *30*, 9329−9338.
(13) Mady, M. F.; Fevang, S.; Kelland, M. A. Study of Novel Aromatic Aminomethylenephosphonates as Oilfield Scale Inhibitors. *Energy Fuels* **2019**, *33*, 228−237.
(14) Mady, M. F.; Charoensumran, P.; Ajiro, H.; Kelland, M. A. Synthesis and Characterization of Modified Aliphatic Polycarbonates as Environmentally Friendly Oilfield Scale Inhibitors. *Energy Fuels* **2018**, *32*, 6746−6755.
(15) Mady, M. F.; Malmin, H.; Kelland, M. A. Sulfonated Nonpolymeric Aminophosphonate Scale Inhibitors-Improving the Compatibility and Biodegradability. *Energy Fuels* **2019**, *33*, 6197−6204.
(16) Mady, M. F.; Bayat, P.; Kelland, M. A. Environmentally Friendly Phosphonated Polyetheramine Scale Inhibitors-Excellent Calcium Compatibility for Oilfield Applications. *Ind. Eng. Chem. Res.* **2020**, *59*, 9808−9818.
(17) Mady, M. F.; Rehman, A.; Kelland, M. A. Synthesis and Antiscaling Evaluation of Novel Hydroxybisphosphonates for Oilfield Applications. *ACS Omega* **2021**, *6*, 6488−6497.
(18) Mady, M. F.; Rehman, A.; Kelland, M. A. Synthesis and Study of Modified Polyaspartic Acid Coupled Phosphonate and Sulfonate Moieties As Green Oilfield Scale Inhibitors. *Ind. Eng. Chem. Res.* **2021**, *60*, 8331−8339.
(19) Zakaria, K.; Salem, A. A.; Ramzi, M. Cost-effective and eco-friendly organophosphorus-based inhibitors for mineral scaling in Egyptian oil reservoirs: Theoretical, experimental and quantum chemical studies. *J. Pet. Sci. Eng.* **2020**, *195*, No. 107519.
(20) Holzner, C.; Ohlendorf, W.; Block, H.-D.; Bertram, H.; Kleinstuck, R.; Moretto, H.-H. Production of 2-Phosphonobutane-1,2,4-tricarboxylic Acid and the Alkali Metal Salts Thereof. US5,639,909, 1997.
(21) Yoeman, A. M.; Harris, A. *Development of an All Organic Ferrous Metal Corrosion Inhibitor*, CORROSION 1986; NACE International Corrosion-86, Paper No. 14; NACE International, 1986; pp 1−6.
(22) Wang, X. Q.; Meng, L. H.; Zhu, H. W.; Liu, L.; Huang, Y. D. Researches on Daqing Oilfield Scale Analysis and Removal Method. *Adv. Mater. Res.* **2012**, *524*−*527*, 1872−1875.
(23) McKenna, C. E.; Levy, J. N.; Khawli, L. A.; Harutunian, V.; Ye, T.-G.; Starnes, M. C.; Bapat, A.; Cheng, Y.-C. Inhibitors of Viral Nucleic Acid Polymerases. *Nucleotide Analogues as Antiviral Agents*; American Chemical Society, 1989; Vol. *401*, pp 1−16.
(24) Organisation for Economic Co-operation and Development (OECD). *Guideline for Testing of Chemicals, Biodegradability in Seawater*; OECD: Paris, France, 1992; p 27.
(25) Rittmann, B. E.; McCarty, P. L. *Environmental Biotechnology: Principles and Applications*; McGraw-Hill, Inc.: Singapore, 2001; p 128.
(26) Ruiz-Agudo, E.; Rodriguez-Navarro, C.; Sebastián-Pardo, E. Sodium Sulfate Crystallization in the Presence of Phosphonates: Implications in Ornamental Stone Conservation. *Cryst. Growth Des.* **2006**, *6*, 1575−1583.
(27) Demadis, K. D.; Lykoudis, P.; Raptis, R. G.; Mezei, G. Phosphonopolycarboxylates as Chemical Additives for Calcite Scale Dissolution and Metallic Corrosion Inhibition Based on a Calcium-Phosphonotricarboxylate Organic- Inorganic Hybrid. *Cryst. Growth Des.* **2006**, *6*, 1064−1067.
(28) Mao, J. C.; Otis, E. R.; von Esch, A. M.; Herrin, T. R.; Fairgrieve, J. S.; Shipkowitz, N. L.; Duff, R. G. Structure-Activity Studies on Phosphonoacetate. *Antimicrob. Agents Chemother.* **1985**, *27*, 197−202.
(29) Chai, J.-D.; Head-Gordon, M. Systematic Optimization of Long-Range Corrected Hybrid Density Functionals. *J. Chem. Phys.* **2008**, *128*, No. 084106.
(30) Grimme, S. Semiempirical GGA-Type Density Functional Constructed with a Long-Range Dispersion Correction. *J. Comput. Chem.* **2006**, *27*, 1787−1799.
(31) Weigend, F.; Ahlrichs, R. Balanced Basis Sets of Split Valence, Triple Zeta Valence and Quadruple Zeta Valence Quality for H to Rn: Design and Assessment of Accuracy. *Phys. Chem. Chem. Phys.* **2005**, *7*, 3297−3305.
(32) Weigend, F. Accurate Coulomb-Fitting Basis Sets for H to Rn. *Phys. Chem. Chem. Phys.* **2006**, *8*, 1057−1065.
(33) Scalmani, G.; Frisch, M. J. Continuous Surface Charge Polarizable Continuum Models of Solvation. I. General Formalism. *J. Chem. Phys.* **2010**, *132*, No. 114110.
(34) Marenich, A. V.; Cramer, C. J.; Truhlar, D. G. Universal Solvation Model Based on Solute Electron Density and on a Continuum Model of the Solvent Defined by the Bulk Dielectric Constant and Atomic Surface Tensions. *J. Phys. Chem. B* **2009**, *113*, 6378−6396.
(35) Frisch, M. J.; Trucks, G. W.; Schlegel, H. B.; Scuseria, G. E.; Robb, M. A.; Cheeseman, J. R.; Scalmani, G.; Barone, V.; Petersson, G. A.; Nakatsuji, H.; Li, X.; Caricato, M.; Marenich, A. V.; Bloino, J.; Janesko, B. G.; Gomperts, R.; Mennucci, B.; Hratchian, H. P.; Ortiz, J. V.; Izmaylov, A. F.; Sonnenberg, J. L.; Williams-Young, D.; Ding, F.; Lipparini, F.; Egidi, F.; Goings, J.; Peng, B.; Petrone, A.; Henderson, T.; Ranasinghe, D.; Zakrzewski, V. G.; Gao, J.; Rega, N.; Zheng, G.; Liang, W.; Hada, M.; Ehara, M.; Toyota, K.; Fukuda, R.; Hasegawa, J.; Ishida, M.; Nakajima, T.; Honda, Y.; Kitao, O.; Nakai, H.; Vreven, T.; Throssell, K.; Montgomery, J. A., Jr.; Peralta, J. E.; Ogliaro, F.; Bearpark, M. J.; Heyd, J. J.; Brothers, E. N.; Kudin, K. N.; Staroverov, V. N.; Keith, T. A.; Kobayashi, R.; Normand, J.; Raghavachari, K.; Rendell, A. P.; Burant, J. C.; Iyengar, S. S.; Tomasi, J.; Cossi, M.; Millam, J. M.; Klene, M.; Adamo, C.; Cammi, R.; Ochterski, J. W.; Martin, R. L.; Morokuma, K.; Farkas, O.; Foresman, J. B.; Fox, D. J. *Gaussian 16*, revision B.01; Gaussian, Inc.: Wallingford, CT, 2016.
(36) Werner, H. J.; Adler, T. B.; Manby, F. R. General Orbital Invariant MP2-F12 Theory. *J. Chem. Phys.* **2007**, *126*, No. 164102.
(37) Simon, S.; Duran, M.; Dannenberg, J. J. How Does Basis Set Superposition Error Change the Potential Surfaces for Hydrogen-Bonded Dimers? *J. Chem. Phys.* **1996**, *105*, 11024−11031.
(38) Kresse, G.; Hafner, J. Ab Initio Molecular Dynamics for Liquid Metals. *Phys. Rev. B* **1993**, *47*, 558.
(39) Kresse, G.; Hafner, J. Ab Initio Molecular-Dynamics Simulation of the Liquid-Metal−Amorphous-Semiconductor Transition in Germanium. *Phys. Rev. B* **1994**, *49*, 14251.

https://doi.org/10.1021/acs.iecr.1c02441
Ind. Eng. Chem. Res. 2021, 60, 12175−12188

(40) Blöchl, P. E. Projector Augmented-Wave Method. *Phys. Rev. B* **1994**, *50*, 17953.
(41) Monkhorst, H. J.; Pack, J. D. Special Points for Brillouin-Zone Integrations. *Phys. Rev. B* **1976**, *13*, 5188.
(42) Perdew, J. P.; Burke, K.; Ernzerhof, M. Generalized Gradient Approximation Made Simple. *Phys. Rev. Lett.* **1996**, *77*, 3865.
(43) (a) Bano, A. M.; Rodger, P. M.; Quigley, D. New Insight into the Stability of CaCO3 Surfaces and Nanoparticles via Molecular Simulation. *Langmuir* **2014**, *30*, 7513−7521. (b) Jones, F.; Richmond, W. R.; Rohl, A. L. Molecular Modeling of Phosphonate Molecules onto Barium Sulfate Terraced Surfaces. *J. Phys. Chem. B* **2006**, *110*, 7414−7424.
(44) Bromley, L. A.; Cottier, D.; Davey, R. J.; Dobbs, B.; Smith, S.; Heywood, B. R. Interactions at the organic/inorganic interface: molecular design of crystallization inhibitors for barite. *Langmuir* **1993**, *9*, 3594−3599.
(45) Hogan, C.; Davies, H.; Robins, L.; Toole, M.; Harris, K. In *Improved Scale Control, Hydrothermal and Environmental Properties with New Maleic Polymer Chemistry Suitable for Downhole Squeeze and Topside Applications*, Chemistry in the Oil Industry XIII: Oilfield Chemistry—New Frontiers, Manchester Conference Centre, U.K., Nov 4−6, 2013.
(46) Fisher, H. C.; Miles, A. F.; Bodnar, S. H.; Fidoe, S. D.; Sitz, C. D. In *Progress towards Biodegradable Phosphonate Scale Inhibitors*, 20th International Oil Field Chemistry Symposium, Geilo, Norway, 2009.
(47) Devarajan, D.; Lian, P.; Brooks, S. C.; Parks, J. M.; Smith, J. C. Quantum Chemical Approach for Calculating Stability Constants of Mercury Complexes. *ACS Earth Space Chem.* **2018**, *2*, 1168−1178.
(48) Jones, F.; Piana, S.; Gale, J. D. Understanding the Kinetics of Barium Sulfate Precipitation from Water and Water−Methanol Solutions. *Cryst. Growth Des.* **2008**, *8*, 817−822.
(49) Spanos, N.; Koutsoukos, P. G. Kinetics of Precipitation of Calcium Carbonate in Alkaline PH at Constant Supersaturation. Spontaneous and Seeded Growth. *J. Phys. Chem. B* **1998**, *102*, 6679−6684.
(50) Leung, W. H.; Nancollas, G. H. Nitrilotri-(methylenephosphonic acid) Adsorption on Barium Sulfate Crystals and Its Influence on Crystal Growth. *J. Cryst. Growth* **1978**, *44*, 163−167.
(51) Tomson, M. B.; Fu, G.; Watson, M. A.; Kan, A. T. Mechanisms of Mineral Scale Inhibition. *SPE Prod. Facil.* **2003**, *18*, 192−199.
(52) Yang, H.; Lou, C.; Sun, L.; Li, J.; Cai, Y.; Wang, Z.; Li, W.; Liu, G.; Tang, Y. admetSAR 2.0: web-service for prediction and optimization of chemical ADMET properties. *Bioinformatics* **2019**, *35*, 1067−1069.

https://doi.org/10.1021/acs.iecr.1c02441
Ind. Eng. Chem. Res. 2021, 60, 12175−12188